Mon. Not. R. Astron. Soc. **000**, 000–000 (0000) Printed 20 January 2013 (MN LaTeX style file v2.2)

The updated luminosity correlations of gamma-ray bursts and cosmological implications

Fa-Yin Wang[1,2⋆], Shi Qi[3,4,5]† & Zi-Gao Dai[1,2]‡
[1] *Department of Astronomy, Nanjing University, Nanjing 210093, China*
[2] *Key Laboratory of Modern Astronomy and Astrophysics (Nanjing University), Ministry of Education, Nanjing 210093, China*
[3] *Purple Mountain Observatory, Chinese Academy of Sciences, Nanjing 210008, China*
[4] *Joint Center for Particle, Nuclear Physics and Cosmology, Nanjing University - Purple Mountain Observatory, Nanjing 210093, China*
[5] *Key Laboratory of Dark Matter and Space Astronomy, Chinese Academy of Sciences.*

20 January 2013

ABSTRACT

Several interesting luminosity correlations among gamma-ray burst (GRB) variables have been recently discussed extensively. In this paper, we derive the six luminosity correlations ($\tau_{\rm lag}-L$, $V-L$, $E_{\rm peak}-L$, $E_{\rm peak}-E_\gamma$, $\tau_{RT}-L$, $E_{\rm peak}-E_{\gamma,\rm iso}$) from the light curves and spectra of the latest 116 long GRBs, including the time lag ($\tau_{\rm lag}$) between low and high photon energy light curves, the variability (V) of the light curve, the peak energy of the spectrum ($E_{\rm peak}$), and the minimum rise time (τ_{RT}) of the peaks. We find that the intrinsic scatter of the $V-L$ correlation is too large and there seems no inherent correlation between the two parameters using the latest GRB data. The other five correlations indeed exist when the sample is enlarged. The $E_{\rm peak}-E_\gamma$ correlation has a significantly lower intrinsic scatter compared to the other correlations. We divide the full data into four redshift bins when testing possible evolution of the correlations with redshift. We find no statistically significant evidence for the redshift evolution of the luminosity correlations. To avoid the circularity problem when constraining the cosmological parameters, we simultaneously minimize χ^2 with respect to both correlation parameters a, b and the cosmological parameters using the maximum likelihood method. For the flat ΛCDM, the best fit is $\Omega_{\rm m}=0.31^{+0.13}_{-0.10}$. We also constrain the possible evolution of the equation of state (EOS) of the dark energy using the GRBs together with the Union2 compilation of SNe Ia and the $H(z)$ data. The result is consistent with the cosmological constant at 2σ confidence level and mainly due to the GRB data, the dark energy EOS shows slight deviation from -1 at $z\geqslant 0.5$ as was persistently presented with many previous data sets.

Key words: cosmology: observations - gamma rays: bursts - cosmology: distance scale - cosmology: cosmological parameters

1 INTRODUCTION

Unexpected accelerating expansion of the universe was first discovered by observing type Ia supernovae (SNe Ia) (Riess et al. 1998; Perlmutter et al. 1999). Independent observations from baryonic acoustic oscillations (BAO) (Eisenstein et al. 2005; Percival et al. 2007), the anisotropy spectrum of cosmic microwave background radiation (Komatsu et al. 2009) and the large scale structure data from large galaxy redshift surveys (Tegmark et al. 2006) have confirmed this surprising result. This acceleration is commonly attributed to dark energy, which is the most mysterious problem in modern cosmology. Among parameters that describe the properties of dark energy, the equation of state (EOS) is one of the most important. Whether and how it evolves with time is crucial in distinguishing different cosmological models. A nearly model-independent approach in which uncorrelated estimates are made about discrete $w(z)$ at different redshifts has been extensively discussed (Huterer & Cooray 2005; Riess et al. 2007; Sullivan et al. 2007; Qi, Wang & Lu 2008).

⋆ fayinwang@nju.edu.cn
† qishi11@gmail.com
‡ dzg@nju.edu.cn

In order to measure the expansion history of our Universe, we need the Hubble diagram of standard candles. SNe Ia are the well known standard candles that have played an important role in constraining cosmological parameters. Unfortunately, it is difficult to observe SNe Ia at $z > 1.7$, even with excellent space based projects such as SNAP (Aldering et al. 2004). They cannot provide any information on the cosmic expansion beyond redshift 1.7. With gamma-ray bursts (GRBs), we can access much higher redshifts. The high luminosities of GRBs make them detectable out to the edge of the visible universe (Lamb & Reichart 2000; Ciardi & Loeb 2000; Bromm & Loeb 2002, 2006). The farthest GRB observed hitherto is GRB 090423 at $z = 8.2$ (Tanvir et al. 2009; Salvaterra et al. 2009). Schaefer (2007) complied 69 GRBs to make simultaneous uses of five luminosity relations, which are the correlations of $\tau_{\rm lag} - L$ (Norris, Marani & Bonnell 2000), $V - L$ (Fenimore & Ramirez-Ruiz 2000), $E_{\rm peak} - L$ (Schaefer et al. 2003; Wei & Gao 2003), $E_{\rm peak} - E_\gamma$(Ghirlanda et al. 2004a), and $\tau_{\rm RT} - L$ (Schaefer 2007). Here the time lag ($\tau_{\rm lag}$) is the time shift between the hard and soft light curves, L is the peak luminosity of a GRB, the variability V of a burst denotes whether its light curve is spiky or smooth and it can be obtained by calculating the normalized variance of an observed light curve around a smoothed version of that light curve (Fenimore & Ramirez- Ruiz 2000), $E_{\rm peak}$ is the photon energy at which the νF_ν spectrum peaks, $E_\gamma = (1 - \cos\theta_j)E_{\gamma,\rm iso}$ is the collimation-corrected energy of a GRB, and the minimum rise time ($\tau_{\rm RT}$) in the gamma-ray light curve is the shortest time over which the light curve rises by half of the peak flux of the pulse. More recently, Yu et al. (2009) found that, for the three-dimensional (3D) luminosity relations between the luminosity and an energy scale $E_{\rm peak}$ and a timescale ($\tau_{\rm lag}$ or τ_{RT}), the intrinsic scatters are considerably smaller than those of corresponding two-dimensional (2D) luminosity relations. Dainotti et al. (2008, 2010) and Qi & Lu (2010) found new correlations between the transition times of the X-ray light curve from exponential to power law and the X-ray luminosities at the transitions. After being calibrated with luminosity relations, GRBs may be used as standard candles to provide information on cosmic expansion at high redshifts and, at the same time, to tighten the constraints on cosmic expansion at low redshifts (Dai et al. 2004; Ghirlanda et al. 2004b; Friedman & Bloom 2005; Liang & Zhang 2005, 2006; Wang & Dai 2006; Schaefer 2007; Wright 2007; Wang, Dai & Zhu 2007; Wang 2008; Qi, Wang & Lu 2008a,b; Liang et al. 2008; Amati et al. 2008; Cardone et al. 2009, 2010; Liang et al. 2009; Qi, Lu & Wang 2009; Izzo et al. 2009; Liang & Zhu 2010). GRBs also can potentially probe the cosmographic parameters to distinguish between dark energy and modified gravity models (Wang, Dai & Qi 2009a, b; Vitagliano et al. 2010; Capozziello & Izzo 2008).

The correlations among GRB variables span a very large range in redshift. Possible evolution effect must be considered when we use these correlations. Li (2007) used the Amati relation ($E_{\rm peak} - E_{\gamma,\rm iso}$) (Amati et al. 2002) as an example to test the cosmic evolution of GRBs and found that the slope of the correlation evolves with the redshift. In contrast, Basilakos & Perivolaropoulos (2008) found no statistically significant evidence for redshift dependence of correlation slopes using 69 GRBs. In this paper, we first enlarge the GRB sample with the new data from Xiao & Schaefer (2009). Our sample includes 116 GRBs ranging from $z = 0.17$ to $z = 8.2$. We divide these GRBs into four redshift bins to investigate the possible evolution effect. Here the focus is on the correlations, so we fix the cosmological parameters. We also use GRBs to constrain the cosmological parameters and dark energy EOS. In order to avoid the circularity problem, we simultaneously fit the correlation parameters and the cosmological parameters.

The structure of this paper is as follows: in the next section we show the latest GRB data and describe our fitting methods. In section 3 we present the updated luminosity correlations and test their redshift dependence. Constraints on cosmological parameters and equation of state of dark energy are presented in section 4. Some conclusions are presented in section 5.

2 OBSERVATIONAL DATA AND ANALYSIS METHOD

The luminosity correlations we will discuss here typically relate a GRB observable with the isotropic peak luminosity L (it is also referenced to as L_p in many papers), the isotropic energy $E_{\gamma,\rm iso}$, or the collimation-corrected energy E_γ. The isotropic peak luminosity is given by

$$L = 4\pi d_L^2 P_{\rm bolo}, \tag{1}$$

the isotropic energy is

$$E_{\gamma,\rm iso} = 4\pi d_L^2 S_{\rm bolo}(1+z)^{-1}, \tag{2}$$

and the collimation-corrected energy is

$$E_\gamma = E_{\gamma,\rm iso}F_{\rm beam} = 4\pi d_L^2 S_{\rm bolo}F_{\rm beam}(1+z)^{-1}. \tag{3}$$

Here, $P_{\rm bolo}$ and $S_{\rm bolo}$ are the bolometric peak flux and fluence, respectively, while $F_{\rm beam} = 1 - \cos\theta_{\rm jet}$ is the beaming factor. From Sari, Piran, & Halpern (1999),

$$\theta_{\rm jet} = 0.161[t_{\rm jet}/(1+z)]^{3/8}(n\ \eta_\gamma/E_{\gamma,\rm iso,52})^{1/8}, \tag{4}$$

where z is the redshift, $t_{\rm jet}$ is the jet break time measured in days, n is the density of the circumburst medium in particles per cubic centimeter, η_γ is the radiative efficiency, and $E_{\gamma,\rm iso,52}$ is the isotropic energy in units of 10^{52} erg for an Earth-facing jet. The jet break time ($t_{\rm jet}$) can be measured when the afterglow brightness has a power-law decline that suddenly steepens due to the slowing down of the jet until the relativistic beaming roughly equals the jet opening angle. In the absence of these detailed fits, we adopt $\eta_\gamma = 0.2$ and $n = 3$ cm^{-3} (Schaefer 2007). Note that $P_{\rm bolo}$ and S_{bolo} are computed from the observed GRB energy spectrum $\Phi(E)$ as follows (Ghirlanda et al. 2004a, Amati 2006):

$$P_{\rm bolo} = P \times \frac{\int_{1/(1+z)}^{10^4/(1+z)} E\Phi(E)dE}{\int_{E_{\rm min}}^{E_{\rm max}} \Phi(E)dE}\ , \tag{5}$$

$$S_{\rm bolo} = S \times \frac{\int_{1/(1+z)}^{10^4/(1+z)} E\Phi(E)dE}{\int_{E_{\rm min}}^{E_{\rm max}} E\Phi(E)dE}\ , \tag{6}$$

with P and S being the observed peak energy and fluence in units of photons/cm^2/s and erg/cm^2, respectively, and $(E_{\rm min}, E_{\rm max})$ the detection thresholds of the observing instrument. For pre-*Swift* GRBs, we take the values of $P_{\rm bolo}$ and $S_{\rm bolo}$ directly from Schaefer (2007). For those GRBs observed by *Swift*, we adopt the values of P and S from *Swift* website [1] and calculate $P_{\rm bolo}$ and $S_{\rm bolo}$ using the above formulae. Concerning the errors of $P_{\rm bolo}$ and $S_{\rm bolo}$ during the calculation, we only take into account the errors propagating from that of P and S. The uncertainties from $\Phi(E)$ are absorbed into intrinsic scatters of the correlations. Note that the energy spectrum is modeled using a smoothly broken power - law (Band et al. 1993),

$$\Phi(E) = \begin{cases} AE^{\alpha}{\rm e}^{-(2+\alpha)E/E_{\rm peak}} & E \leqslant \frac{\alpha-\beta}{2+\alpha}E_{\rm peak} \\ \\ BE^{\beta} & \text{otherwise} \end{cases} \tag{7}$$

where α is the asymptotic power-law index for photon energies below the break and β is the power-law index for photon energies above the break. We use the values of α and β from Xiao & Schaefer (2009). The luminosity correlations are power-law relations of either L, $E_{\gamma,{\rm iso}}$ or E_γ as a function of $\tau_{\rm lag}$, V, $E_{\rm peak}$, or τ_{RT}. The luminosity indicators of $\tau_{\rm lag}$, V, $E_{\rm peak}$, and τ_{RT} are also directly taken from Xiao & Schaefer (2009). L, $E_{\gamma,{\rm iso}}$, and E_γ depend not only on the GRB observables $P_{\rm bolo}$ or $S_{\rm bolo}$, but also on the cosmological parameters through the luminosity distance d_L, which in a flat universe is expressed in terms of the Hubble expansion rate $H(z) = H_0E(z)$ as

$$d_L(\Omega_{\rm m}, z) = (1+z)\frac{c}{H_0}\int_0^z \frac{dz'}{E(z')}, \tag{8}$$

where $E^2(z) = \Omega_{\rm m}(1+z)^3 + \Omega_{\rm x}f_{\rm x}(z)$ and the dimensionless dark energy density $f_{\rm x}(z)$ is given by ($w(z)$ is the EOS of dark energy)

$$f_{\rm x}(z) = \exp\left[3\int_0^z \frac{1+w(\tilde z)}{1+\tilde z}{\rm d}\tilde z\right]. \tag{9}$$

When the focus is on the luminosity correlations themselves, the cosmological parameters here are fixed.

The luminosity correlations involved in this paper are

$$\log\frac{L}{1\ {\rm erg\ s^{-1}}} = a_1 + b_1\log\left[\frac{\tau_{\rm lag}(1+z)^{-1}}{0.1\ {\rm s}}\right], \tag{10}$$

$$\log\frac{L}{1\ {\rm erg\ s^{-1}}} = a_2 + b_2\log\left[\frac{V(1+z)}{0.02}\right], \tag{11}$$

$$\log\frac{L}{1\ {\rm erg\ s^{-1}}} = a_3 + b_3\log\left[\frac{E_{\rm peak}(1+z)}{300\ {\rm keV}}\right], \tag{12}$$

$$\log\frac{E_\gamma}{1\ {\rm erg}} = a_4 + b_4\log\left[\frac{E_{\rm peak}(1+z)}{300\ {\rm keV}}\right], \tag{13}$$

$$\log\frac{L}{1\ {\rm erg\ s^{-1}}} = a_5 + b_5\log\left[\frac{\tau_{\rm RT}(1+z)^{-1}}{0.1\ {\rm s}}\right], \tag{14}$$

$$\log\frac{E_{\gamma,{\rm iso}}}{1\ {\rm erg}} = a_6 + b_6\log\left[\frac{E_{\rm peak}(1+z)}{300\ {\rm keV}}\right]. \tag{15}$$

Concerning the luminosity indicators in the correlations, for the temporal indicators, the observed quantities must be divided by $1+z$ to correct the time dilation. The observed V-value must be multiplied by $1+z$ because it varies inversely with time, and the observed $E_{\rm peak}$ must be multiplied by $1+z$ to correct the redshift dilation of the spectrum.

The first five of the correlations listed above were the ones considered in Schaefer (2007) and Xiao & Schaefer (2009). We add in our analysis the investigation of the Amati correlation ($E_{\rm peak} - E_{\gamma,{\rm iso}}$), which was initially discovered on a small sample of BeppoSAX GRBs with known redshift (Amati et al. 2002) and confirmed afterwards by Swift observations (Amati 2006). Compared to the $E_{\rm peak} - E_\gamma$ correlation, due to the independence of $\theta_{\rm jet}$, the $E_{\rm peak} - E_{\gamma,{\rm iso}}$ correlation can be used for almost the whole GRB sample and does not suffer from the assumptions and uncertainties around $\theta_{\rm jet}$ that affect the $E_{\rm peak} - E_\gamma$ correlation. Also, compared to the $E_{\rm peak} - L$ correlation, the $E_{\rm peak} - E_{\gamma,{\rm iso}}$ correlation is not affected by assumptions on the peak flux time scale and on the spectral shape at the peak (i.e., the peak luminosity is always computed by assuming the spectral shape of the time-averaged spectrum, which is not physical, given that the spectrum at the peak is often much different than the average one). There is also debate about the reality of these correlations, see Nakar & Piran (2005), Band & Preece 2005, Butler et al. (2007), Butler et al. (2009), Ghirlanda et al. (2005), Bosnjak et al. (2008), Ghirlanda et al. (2008), Nava et al. (2008), Krimm et al. (2009), Amati et al. (2009), Ghirlanda et al. (2010) etc.

In Table 1, we list the variables of 116 GRBs that we use in fitting luminosity correlations. In addition to the GRBs included in the analysis of Xiao & Schaefer (2009), we add the GRB090423, which has the highest redshift so far. We use the typical spectral index $\alpha = -1$ and $\beta = -2.2$ for this burst (Salvaterra et al. 2009).

[1] See http://swift.gsfc.nasa.gov/docs/swift/archive/grb_table.

GRB	z	$P_{\rm bolo}$ [erg/cm^{2}s]	$S_{\rm bolo}$ [erg/cm^2]	$F_{\rm beam}$	τ_{lag} [sec]	V	$E_{\rm peak}$ [keV]	τ_{RT} [sec]
970228	0.70	7.3E-6 ± 4.3E-7	···	···	···	0.016 ± 0.010	115^{+38}_{-38}	···
970508	0.84	3.3E-6 ± 3.3E-7	8.09E-6 ± 8.1E-7	0.0795 ± 0.0204	0.49 ± 0.02	0.018 ± 0.004	389^{+40}_{-40}	0.65 ± 0.07
970828	0.96	1.0E-5 ± 1.1E-6	1.23E-4 ± 1.2E-5	5.32E-03 ± 1.44E-03	···	0.052 ± 0.005	298^{+30}_{-30}	0.36 ± 0.14
971214	3.42	7.5E-7 ± 2.4E-8	···	···	0.03 ± 0.05	0.048 ± 0.002	190^{+20}_{-20}	···
980703	0.97	1.2E-6 ± 3.6E-8	2.83E-5 ± 2.9E-6	1.84E-02 ± 2.67E-03	0.69 ± 0.02	0.024 ± 0.001	254^{+25}_{-25}	3.00 ± 0.19
990123	1.61	1.3E-5 ± 5.0E-7	3.11E-4 ± 3.1E-5	2.41E-03 ± 6.90E-04	0.07 ± 0.01	0.059 ± 0.003	604^{+60}_{-60}	···
990506	1.31	1.1E-5 ± 1.5E-7	···	···	0.04 ± 0.01	0.337 ± 0.001	283^{+30}_{-30}	0.13 ± 0.01
990510	1.62	3.3E-6 ± 1.2E-7	2.85E-5 ± 2.9E-6	2.13E-03 ± 3.19E-04	0.03 ± 0.01	0.118 ± 0.001	126^{+10}_{-10}	0.13 ± 0.01
990705	0.84	6.6E-6 ± 2.6E-7	1.34E-4 ± 1.5E-5	3.48E-03 ± 9.60E-04	···	0.097 ± 0.004	189^{+15}_{-15}	0.62 ± 0.37
991208	0.71	2.1E-5 ± 2.1E-6	···	···	···	0.023 ± 0.003	190^{+20}_{-20}	0.27 ± 0.01
991216	1.02	4.1E-5 ± 3.8E-7	2.48E-4 ± 2.5E-5	3.00E-03 ± 9.46E-04	0.03 ± 0.01	0.062 ± 0.003	318^{+30}_{-30}	0.09 ± 0.01
000131	4.50	7.3E-7 ± 8.3E-8	···	···	···	0.056 ± 0.005	163^{+13}_{-13}	0.84 ± 0.39
000210	0.85	2.0E-5 ± 2.1E-6	···	···	···	0.018 ± 0.002	408^{+14}_{-14}	0.45 ± 0.03
000911	1.06	1.9E-5 ± 1.9E-6	···	···	···	0.122 ± 0.013	986^{+100}_{-100}	0.07 ± 0.22
000926	2.07	2.9E-6 ± 2.9E-7	···	···	···	0.326 ± 0.034	100^{+7}_{-7}	···
010222	1.48	2.3E-5 ± 7.2E-7	2.45E-4 ± 9.1E-6	0.0014 ± 0.0001	···	0.143 ± 0.004	309^{+12}_{-12}	0.45 ± 0.01
010921	0.45	1.8E-6 ± 1.6E-7	···	···	1.00 ± 0.04	0.008 ± 0.006	89^{+22}_{-14}	4.31 ± 0.71
020124	3.20	6.1E-7 ± 1.0E-7	1.14E-5 ± 1.1E-6	4.10E-03 ± 1.09E-03	0.07 ± 0.06	0.266 ± 0.040	87^{+18}_{-12}	0.59 ± 0.17
020405	0.70	7.4E-6 ± 3.1E-7	1.10E-4 ± 2.1E-6	5.98E-03 ± 1.96E-03	···	0.104 ± 0.007	364^{+90}_{-90}	0.48 ± 0.09
020813	1.25	3.8E-6 ± 2.6E-7	1.59E-4 ± 2.9E-6	1.14E-03 ± 2.92E-04	0.15 ± 0.01	0.164 ± 0.004	140^{+14}_{-13}	0.59 ± 0.05
021004	2.32	2.3E-7 ± 5.5E-8	3.61E-6 ± 8.6E-7	1.04E-02 ± 2.56E-03	0.71 ± 0.19	0.035 ± 0.067	80^{+53}_{-23}	1.23 ± 0.96
021211	1.01	2.3E-6 ± 1.7E-7	···	···	0.31 ± 0.01	0.006 ± 0.003	46^{+8}_{-6}	0.57 ± 0.01
030115	2.50	3.2E-7 ± 5.1E-8	···	···	0.44 ± 0.06	0.020 ± 0.020	83^{+53}_{-22}	0.70 ± 0.40
030226	1.98	2.6E-7 ± 4.7E-8	8.33E-6 ± 9.8E-7	2.72E-03 ± 6.82E-04	0.31 ± 0.22	0.033 ± 0.029	97^{+27}_{-17}	1.76 ± 1.15
030323	3.37	1.2E-7 ± 6.0E-8	···	···	···	0.021 ± 0.338	44^{+90}_{-26}	···
030328	1.52	1.6E-6 ± 1.1E-7	6.14E-5 ± 2.4E-6	1.96E-03 ± 4.92E-04	0.08 ± 0.08	0.024 ± 0.003	130^{+14}_{-13}	1.69 ± 0.81
030329	0.17	2.0E-5 ± 1.0E-6	2.31E-4 ± 2.0E-6	4.89E-03 ± 8.62E-04	0.15 ± 0.01	0.065 ± 0.002	68^{+2}_{-2}	0.66 ± 0.01
030429	2.66	2.0E-7 ± 5.4E-8	1.13E-6 ± 1.9E-7	5.76E-03 ± 2.79E-03	0.03 ± 0.17	0.220 ± 0.135	35^{+12}_{-8}	···
030528	0.78	1.6E-7 ± 3.2E-8	···	···	12.56 ± 0.14	0.017 ± 0.010	32^{+5}_{-5}	2.13 ± 0.42
040924	0.86	2.6E-6 ± 2.8E-7	···	···	0.90 ± 0.01	0.060 ± 0.003	67^{+6}_{-6}	0.33 ± 0.17
041006	0.71	2.5E-6 ± 1.4E-7	1.75E-5 ± 1.8E-6	1.13E-03 ± 3.40E-04	···	0.050 ± 0.002	63^{+13}_{-13}	1.28 ± 0.01
050126	1.29	1.07E-07 ± 1.56E-08	1.99E-06 ± 1.15E-07	···	2.74 ± 0.02	-0.010 ± 0.065	47^{+23}_{-8}	1.58 ± 1.91
050223	0.59	1.18E-07 ± 1.66E-08	1.68E-06 ± 1.04E-07	···	···	0.111 ± 0.094	62^{+10}_{-10}	···
050315	1.95	2.79E-07 ± 1.93E-08	7.52E-06 ± 2.07E-07	···	···	0.032 ± 0.016	39^{+7}_{-7}	1.97 ± 1.62
050401	2.90	1.74E-06 ± 9.09E-08	1.69E-05 ± 3.83E-07	2.20E-03 ± 7.52E-04	0.06 ± 0.02	0.187 ± 0.019	118^{+18}_{-18}	0.25 ± 0.16
050406	2.44	4.05E-08 ± 6.84E-09	1.41E-07 ± 1.77E-08	···	···	0.020 ± 0.274	25^{+35}_{-13}	···
050408	1.24	1.1E-6 ± 2.1E-7	···	···	0.31 ± 0.02	0.082 ± 0.005	100^{+100}_{-50}	0.49 ± 0.02
050416A	0.65	5.41E-07 ± 3.24E-08	9.28E-07 ± 5.68E-08	1.45E-02 ± 8.38E-03	···	0.021 ± 0.030	15^{+2}_{-3}	0.54 ± 0.06
050505	4.27	2.94E-07 ± 2.99E-08	5.23E-06 ± 2.29E-07	···	0.71 ± 0.13	0.076 ± 0.031	70^{+140}_{-24}	0.60 ± 0.21
050525A	0.61	4.74E-06 ± 6.50E-08	2.44E-05 ± 2.14E-07	2.47E-03 ± 8.46E-04	0.12 ± 0.01	0.093 ± 0.003	81^{+1}_{-1}	0.32 ± 0.01
050603	2.82	8.01E-06 ± 2.42E-07	2.73E-05 ± 5.98E-07	···	-0.01 ± 0.01	0.125 ± 0.014	344^{+52}_{-52}	0.19 ± 0.01
050730	3.97	1.02E-07 ± 1.58E-08	5.80E-06 ± 2.25E-07	···	···	0.027 ± 0.066	124^{+26}_{-26}	···
050802	1.71	5.47E-07 ± 5.32E-08	5.24E-06 ± 2.50E-07	···	···	0.070 ± 0.036	121^{+28}_{-28}	2.03 ± 1.02
050814	5.30	1.04E-07 ± 2.24E-08	3.99E-06 ± 2.65E-07	···	···	-0.009 ± 0.180	60^{+24}_{-6}	···
050820A	2.61	6.12E-07 ± 3.49E-08	1.09E-05 ± 4.66E-07	6.73E-03 ± 3.09E-03	···	0.061 ± 0.033	246^{+76}_{-40}	1.01 ± 0.75
050824	0.83	7.92E-08 ± 1.44E-08	7.41E-07 ± 8.81E-08	···	···	0.289 ± 0.640	15^{+5}_{-5}	···
050826	0.30	7.66E-08 ± 1.59E-08	1.12E-06 ± 1.19E-07	···	···	0.063 ± 0.105	105^{+47}_{-47}	1.11 ± 2.28
050908	3.35	9.83E-08 ± 1.20E-08	1.09E-06 ± 6.98E-08	···	···	-0.017 ± 0.046	41^{+9}_{-5}	1.10 ± 1.47
050922C	2.20	1.93E-06 ± 5.18E-08	5.09E-06 ± 1.03E-07	···	0.06 ± 0.01	0.015 ± 0.003	198^{+38}_{-22}	0.13 ± 0.01
051016B	0.94	1.92E-07 ± 1.43E-08	4.31E-07 ± 3.39E-08	···	···	0.008 ± 0.030	24^{+7}_{-7}	···
051022	0.80	1.1E-5 ± 8.7E-7	3.40E-4 ± 1.2E-5	0.0029 ± 0.0001	···	0.088 ± 0.008	510^{+22}_{-20}	0.19 ± 0.04
051109A	2.35	8.30E-07 ± 8.83E-08	6.10E-06 ± 4.58E-07	···	···	-0.006 ± 0.025	161^{+130}_{-35}	0.70 ± 1.25
051111	1.55	7.61E-07 ± 3.65E-08	1.38E-05 ± 2.76E-07	···	1.70 ± 0.07	0.009 ± 0.004	220^{+1703}_{-48}	1.80 ± 0.24
060108	2.03	1.22E-07 ± 1.16E-08	8.62E-07 ± 5.26E-08	···	···	0.006 ± 0.040	65^{+600}_{-10}	···
060115	3.53	1.30E-07 ± 1.09E-08	3.76E-06 ± 2.01E-07	···	···	0.019 ± 0.029	62^{+19}_{-6}	1.11 ± 1.71
060206	4.05	4.41E-07 ± 1.63E-08	1.90E-06 ± 5.83E-08	···	0.01 ± 0.03	0.007 ± 0.004	78^{+23}_{-8}	1.16 ± 0.18
060210	3.91	5.37E-07 ± 3.36E-08	1.97E-05 ± 6.39E-07	···	0.15 ± 0.17	0.183 ± 0.033	149^{+400}_{-35}	0.73 ± 0.50
060223A	4.41	2.06E-07 ± 1.67E-08	1.51E-06 ± 6.54E-08	···	···	0.036 ± 0.021	71^{+100}_{-10}	0.41 ± 0.23
060418	1.49	1.49E-06 ± 4.85E-08	2.62E-05 ± 4.85E-07	···	0.22 ± 0.03	0.104 ± 0.008	230^{+20}_{-20}	0.67 ± 0.08
060502A	1.51	3.72E-07 ± 2.81E-08	6.59E-06 ± 1.77E-07	···	4.90 ± 0.11	0.004 ± 0.010	156^{+400}_{-33}	2.94 ± 1.19
060510B	4.90	9.51E-08 ± 1.12E-08	9.98E-06 ± 2.62E-07	···	···	0.110 ± 0.060	95^{+60}_{-30}	···

GRB	z	$P_{\rm bolo}$ [erg/cm^{2}s]	$S_{\rm bolo}$ [erg/cm^2]	$F_{\rm beam}$	τ_{lag} [sec]	V	$E_{\rm peak}$ [keV]	τ_{RT} [sec]
060512	0.44	1.32E-07 ± 1.83E-08	6.04E-07 ± 6.34E-08	···	···	0.043 ± 0.173	22^{+6}_{-6}	···
060522	5.11	8.73E-08 ± 1.45E-08	2.42E-06 ± 1.43E-07	···	···	0.034 ± 0.185	80^{+382}_{-12}	···
060526	3.21	2.33E-07 ± 1.53E-08	3.01E-06 ± 2.40E-07	6.55E-03 ± 1.60E-03	0.17 ± 0.09	0.085 ± 0.030	25^{+5}_{-5}	0.38 ± 0.11
060604	2.68	5.10E-08 ± 1.19E-08	9.82E-07 ± 1.57E-07	···	···	0.080 ± 0.338	40^{+5}_{-5}	···
060605	3.80	8.56E-08 ± 1.36E-08	1.58E-06 ± 1.24E-07	8.23E-04 ± 5.14E-05	···	-0.013 ± 0.068	90^{+91}_{-12}	1.22 ± 0.72
060607A	3.08	2.66E-07 ± 1.50E-08	6.33E-06 ± 1.69E-07	···	1.98 ± 0.11	0.025 ± 0.008	120^{+190}_{-17}	1.23 ± 0.68
060707	3.43	1.53E-07 ± 2.12E-08	3.41E-06 ± 1.96E-07	···	···	0.050 ± 0.054	63^{+13}_{-6}	···
060714	2.71	2.30E-07 ± 1.42E-08	6.88E-06 ± 2.47E-07	···	···	0.125 ± 0.022	103^{+21}_{-16}	···
060729	0.54	1.93E-07 ± 1.30E-08	6.43E-06 ± 3.16E-07	···	···	0.092 ± 0.041	61^{+9}_{-9}	···
060814	0.84	1.83E-06 ± 4.44E-08	4.94E-05 ± 4.91E-07	···	0.29 ± 0.03	0.040 ± 0.003	257^{+74}_{-35}	1.65 ± 0.24
060904B	0.70	4.37E-07 ± 2.28E-08	4.05E-06 ± 2.17E-07	···	0.36 ± 0.09	0.003 ± 0.008	80^{+770}_{-12}	1.00 ± 0.16
060908	2.43	6.69E-07 ± 3.36E-08	7.68E-06 ± 1.85E-07	···	0.26 ± 0.06	0.061 ± 0.008	151^{+112}_{-25}	0.52 ± 0.09
060926	3.21	1.56E-07 ± 1.22E-08	5.47E-07 ± 3.80E-08	···	1.03 ± 0.11	0.148 ± 0.050	20^{+11}_{-11}	···
060927	5.60	4.02E-07 ± 1.54E-08	2.37E-06 ± 8.67E-08	···	0.12 ± 0.04	0.094 ± 0.010	72^{+15}_{-7}	0.46 ± 0.12
061007	1.26	7.20E-06 ± 1.11E-07	2.24E-04 ± 1.72E-06	···	0.11 ± 0.01	0.066 ± 0.003	399^{+12}_{-11}	0.38 ± 0.02
061110A	0.76	9.79E-08 ± 1.35E-08	2.71E-06 ± 1.18E-07	···	···	-0.038 ± 0.050	90^{+13}_{-13}	···
061110B	3.44	1.79E-07 ± 2.66E-08	6.12E-06 ± 3.38E-07	···	0.24 ± 0.36	0.155 ± 0.064	517^{+53}_{-53}	0.79 ± 0.64
061121	1.31	8.04E-06 ± 1.07E-07	6.53E-05 ± 5.76E-07	···	0.03 ± 0.01	0.050 ± 0.003	606^{+55}_{-44}	0.98 ± 0.19
061222B	3.36	2.29E-07 ± 3.15E-08	5.01E-06 ± 2.49E-07	···	···	0.024 ± 0.043	49^{+8}_{-8}	···
070110	2.35	1.12E-07 ± 1.36E-08	4.04E-06 ± 1.64E-07	···	···	-0.010 ± 0.031	110^{+30}_{-30}	···
070208	1.17	1.39E-07 ± 2.06E-08	1.06E-06 ± 1.46E-07	···	···	0.083 ± 0.211	51^{+10}_{-10}	···
070318	0.84	4.10E-07 ± 2.12E-08	7.34E-06 ± 2.01E-07	···	···	0.037 ± 0.008	154^{+19}_{-19}	0.72 ± 0.24
070411	2.95	1.50E-07 ± 1.31E-08	6.29E-06 ± 2.19E-07	···	···	0.041 ± 0.029	83^{+11}_{-11}	···
070506	2.31	1.67E-07 ± 1.38E-08	5.16E-07 ± 3.43E-08	···	2.52 ± 0.04	0.010 ± 0.030	31^{+2}_{-3}	0.12 ± 0.06
070508	0.82	7.67E-06 ± 1.18E-07	7.26E-05 ± 6.15E-07	···	0.04 ± 0.01	0.106 ± 0.003	233^{+7}_{-7}	0.20 ± 0.01
070521	0.55	2.09E-06 ± 5.26E-08	2.97E-05 ± 4.00E-07	···	0.04 ± 0.01	0.116 ± 0.004	222^{+16}_{-12}	0.58 ± 0.06
070529	2.50	3.32E-07 ± 5.08E-08	7.44E-06 ± 4.31E-07	···	···	0.170 ± 0.091	180^{+52}_{-52}	···
070611	2.04	1.45E-07 ± 2.25E-08	9.52E-07 ± 8.44E-08	···	···	0.053 ± 0.080	92^{+30}_{-30}	···
070612A	0.62	2.77E-07 ± 4.24E-08	2.72E-05 ± 9.37E-07	···	···	0.032 ± 0.023	87^{+17}_{-17}	2.49 ± 1.48
070714B	0.92	3.24E-06 ± 1.46E-07	8.91E-06 ± 6.77E-07	···	0.03 ± 0.01	0.164 ± 0.021	1120^{+473}_{-230}	0.45 ± 0.04
070802	2.45	6.38E-08 ± 9.69E-09	6.50E-07 ± 7.05E-08	···	···	-0.156 ± 0.150	70^{+25}_{-25}	···
070810A	2.17	2.77E-07 ± 1.77E-08	1.59E-06 ± 8.43E-08	···	1.09 ± 0.23	-0.006 ± 0.015	44^{+9}_{-9}	0.73 ± 0.22
071003	1.10	4.71E-06 ± 1.82E-07	6.73E-05 ± 1.48E-06	···	0.38 ± 0.05	0.072 ± 0.007	799^{+75}_{-61}	0.88 ± 0.07
071010A	0.98	1.17E-07 ± 2.67E-08	4.97E-07 ± 6.05E-08	···	···	-0.076 ± 0.153	27^{+10}_{-10}	···
071010B	0.95	9.20E-07 ± 2.18E-08	8.37E-06 ± 1.16E-07	···	0.84 ± 0.04	0.010 ± 0.003	52^{+6}_{-8}	1.21 ± 0.03
071031	2.69	7.08E-08 ± 8.61E-09	2.19E-06 ± 1.92E-07	···	···	-0.038 ± 0.108	24^{+7}_{-7}	···
071117	1.33	2.71E-06 ± 5.83E-08	7.97E-06 ± 2.02E-07	···	0.60 ± 0.01	0.009 ± 0.003	278^{+143}_{-48}	0.20 ± 0.02
071122	1.14	6.76E-08 ± 2.06E-08	1.41E-06 ± 1.63E-07	···	···	0.391 ± 0.392	73^{+30}_{-30}	···
080210	2.64	2.57E-07 ± 1.95E-08	4.17E-06 ± 1.41E-07	···	0.53 ± 0.17	0.019 ± 0.013	73^{+15}_{-15}	0.57 ± 0.44
080310	2.43	1.83E-07 ± 1.72E-08	5.49E-06 ± 2.90E-07	···	···	0.038 ± 0.021	28^{+6}_{-6}	0.41 ± 0.55
080319B	0.94	1.55E-05 ± 1.91E-07	5.25E-04 ± 3.94E-06	···	0.02 ± 0.01	0.031 ± 0.003	651^{+8}_{-8}	0.14 ± 0.01
080319C	1.95	2.22E-06 ± 7.79E-08	1.77E-05 ± 2.99E-07	···	···	0.042 ± 0.007	307^{+85}_{-56}	0.21 ± 0.12
080330	1.51	1.33E-07 ± 1.80E-08	8.77E-07 ± 1.26E-07	···	···	0.109 ± 0.060	20^{+9}_{-9}	···
080411	1.03	1.04E-05 ± 1.31E-07	8.75E-05 ± 2.01E-07	···	0.21 ± 0.01	0.167 ± 0.003	259^{+21}_{-16}	0.65 ± 0.01
080413A	2.43	1.22E-06 ± 2.65E-08	9.86E-06 ± 1.71E-07	···	0.13 ± 0.03	0.078 ± 0.004	170^{+48}_{-24}	0.23 ± 0.03
080413B	1.10	3.17E-06 ± 8.25E-08	8.00E-06 ± 1.52E-07	···	0.23 ± 0.01	0.004 ± 0.003	73^{+10}_{-10}	0.50 ± 0.03
080430	0.77	4.60E-07 ± 2.15E-08	3.01E-06 ± 1.53E-07	···	0.68 ± 0.08	0.009 ± 0.004	80^{+15}_{-15}	0.76 ± 0.12
080516	3.20	2.77E-07 ± 2.80E-08	5.88E-07 ± 5.50E-08	···	0.15 ± 0.01	0.168 ± 0.055	66^{+24}_{-24}	···
080520	1.55	8.23E-08 ± 1.00E-08	1.59E-07 ± 3.00E-08	···	···	0.037 ± 0.098	12^{+5}_{-5}	···
080603B	2.69	7.57E-07 ± 2.63E-08	7.02E-06 ± 1.78E-07	···	0.08 ± 0.01	0.283 ± 0.010	85^{+55}_{-18}	0.22 ± 0.03
080605	1.64	5.99E-06 ± 1.10E-07	4.72E-05 ± 4.32E-07	···	0.11 ± 0.01	0.057 ± 0.003	246^{+14}_{-11}	0.22 ± 0.01
080607	3.04	8.35E-06 ± 2.42E-07	1.00E-04 ± 0.00E+00	···	0.04 ± 0.01	0.035 ± 0.003	394^{+35}_{-33}	0.18 ± 0.06
080707	1.23	1.68E-07 ± 1.02E-08	1.26E-06 ± 8.87E-08	···	···	0.093 ± 0.032	73^{+20}_{-20}	···
080721	2.60	9.57E-06 ± 5.01E-07	5.99E-05 ± 3.04E-06	···	0.13 ± 0.05	0.048 ± 0.009	485^{+41}_{-36}	0.09 ± 0.04
090423	8.2	2.17E-07 ± 1.55E-08	1.15E-06 ± 4.73E-08	···	···	···	$48.6^{+3.8}_{-3.8}$	···

Table 1: The data of 116 GRBs used in our analysis. For pre-*Swift* GRBs, we take the values of $P_{\rm bolo}$ and $S_{\rm bolo}$ directly from Schaefer (2007). For those GRBs observed by *Swift*, we adopt the values of P and S from *Swift* website and calculate $P_{\rm bolo}$ and $S_{\rm bolo}$. We use the $F_{\rm beam}$ value from Ghirlanda et al. (2007). Other data are taken from Xiao & Schaefer (2009).

The six luminosity relations can be expressed, in general, as $R = AQ^b$ and Eq. (10)-(15) are the corresponding logarithm forms

$$\log R = \log A + b \log Q \Rightarrow y = a + bx. \tag{16}$$

For the fit of this linear relation, we used the techniques presented in D'Agostini (2005), according to which, the joint likelihood function for the coefficients a and b and the intrinsic scatter $\sigma_{\rm int}$ is

$$L(a, b, \sigma_{\rm int}) \propto \prod_i \frac{1}{\sqrt{\sigma_{\rm int}^2 + \sigma_{y_i}^2 + b^2\sigma_{x_i}^2}} \times \exp[-\frac{(y_i - a - bx_i)^2}{2(\sigma_{\rm int}^2 + \sigma_{y_i}^2 + b^2\sigma_{x_i}^2)}] \tag{17}$$

where x_i and y_i are corresponding observational data for the ith GRB. When considering error propagation from a quantity, say ξ with error σ_ξ, to its logarithm, we set $\frac{\log(\xi+\sigma_\xi^+)+\log(\xi-\sigma_\xi^-)}{2}$ and $\frac{\log(\xi+\sigma_\xi^+)-\log(\xi-\sigma_\xi^-)}{2}$ as the center value and the error of the logarithm correspondingly. This requires $\xi > \sigma_\xi^-$ (the quantities we are interested in here are all positive). Due to the limitation of the data, for a given luminosity correlation, not all the GRBs have all of the needed observational quantities available and satisfy $\xi > \sigma_\xi^-$ at the same time. The numbers of GRBs for each fit of the luminosity correlations are included in Table 2.

3 TEST OF THE UPDATED LUMINOSITY CORRELATIONS

3.1 Luminosity correlations

Our fitting results for the six luminosity correlations are shown in Figure 1 and the last column of Table 2. We assume a flat ΛCDM with $\Omega_{\rm m} = 0.27$ and $H_0 = 70$ km s^{-1}Mpc^{-1} obtained from the five years WMAP data (Komatsu et al. 2009). The best-fit line and 2σ confidence region are plotted in Figure 1.

From Figure 1, we can see that the $E_{\rm peak} - E_\gamma$ correlation is the tightest one. The $V - L$ relation is quite scattered. Its intrinsic scatter ($\sigma_{\rm int} = 0.67$) has been larger than the one that could be expected for a linear relation.

3.2 Test redshift variation of correlations

In order to test if the correlations discussed in the above section vary with redshift, we divide the GRB samples into four groups corresponding to the following redshift bins: $z \in [0, 1]$, $z \in (1, 2]$, $z \in (2, 3]$ and $z \in (3, 8.5]$. For each correlation and each redshift bin, we perform the same fit procedure as applied to the whole GRB sample to determine the parameters a, b and the intrinsic scatter $\sigma_{\rm int}$. The results of the fits and the number of GRBs used in each fit are summarized in Table 2.

For further analysis, we perform linear fits to the parameters a and b versus redshift (the redshifts for the parameters a and b are calculated just by averaging the redshifts of the GRBs used in deriving corresponding a and b). These fits are shown in Figure 2 and the slopes of a and b versus redshift are presented in Table 3. For the $E_{\rm peak} - E_\gamma$ correlation, there are no enough GRB samples to perform such fits. For the other luminosity correlations except for $E_{\rm peak} - L$, the slopes of b versus redshift are all consistent with zero at the 2σ confidence level, and even for $E_{\rm peak} - L$ correlation, zero is near the edge of the 2σ confidence interval of the slope of b versus redshift. Considering that, for the redshifts corresponding to a and b, we only loosely use the average values of the redshifts of corresponding GRBs and the uncertainties in the redshifts are not taken into account (which leads to an underestimate of the uncertainties in the slopes), we can conclude that there is no statistically significant evidence for the evolution of the luminosity correlations with redshift. We didn't take into account the redshift evolution of the parameters a when drawing the conclusion, since they correspond to normalization factors in the luminosity correlations and a small change in b may lead to a larger change in a. In fact, as can be seen from Table 3, the slopes of a versus redshift for the first three luminosity correlations considerably deviate from zero.

4 CONSTRAINTS ON COSMOLOGICAL PARAMETERS AND DARK ENERGY EQUATION OF STATE

To constrain the cosmological parameters, we simultaneously fit correlation parameters of GRBs and cosmological parameters to avoid the circularity problem. Since the luminosity correlations of $E_{\rm peak} - E_\gamma$ and $E_{\rm peak} - E_{\gamma,\rm iso}$ describe almost the same physics, we can only include one of them in the fit to avoid strong correlation among the luminosity correlations. We choose the $E_{\rm peak} - E_\gamma$ correlation, which has a smaller intrinsic scatter. Since the intrinsic scatter of the $V - L$ correlation has been too large, including it in the fit or not has little effect on the result. For the flat ΛCDM model, the combination of the correlations gives the result of $\Omega_{\rm m} = 0.31^{+0.13}_{-0.10}$. Schaefer (2007) used a combination of the same correlations with a smaller sample of GRBs and got the result of $\Omega_{\rm m} \simeq 0.39$. Our result is consistent with the value of Schaefer (2007) at the 1σ confidence level.

We also constrain the dark energy EOS using the GRBs together with SNe Ia and the $H(z)$ data. We adopt the redshift binned parametrization for the dark energy EOS, as proposed in Huterer & Cooray (2005), in which the redshifts are divided into several bins and the dark energy EOS is taken to be constant in each redshift bin but can vary from bin to bin. For this parametrization, $f(z) = \rho_{\rm DE}(z)/\rho_{\rm DE}(0)$ takes the form (Sullivan et al. 2007)

$$f(z_{n-1} < z \leqslant z_n) = (1+z)^{3(1+w_n)} \prod_{i=0}^{n-1} (1+z_i)^{3(w_i - w_{i+1})}, \tag{18}$$

where w_i is the EOS parameter in the $i^{\rm th}$ redshift bin defined by an upper boundary at z_i, and the zeroth bin is defined as $z_0 = 0$. Such a parametrization scheme assumes less about the nature of the dark energy, especially at high redshift, compared with other simple

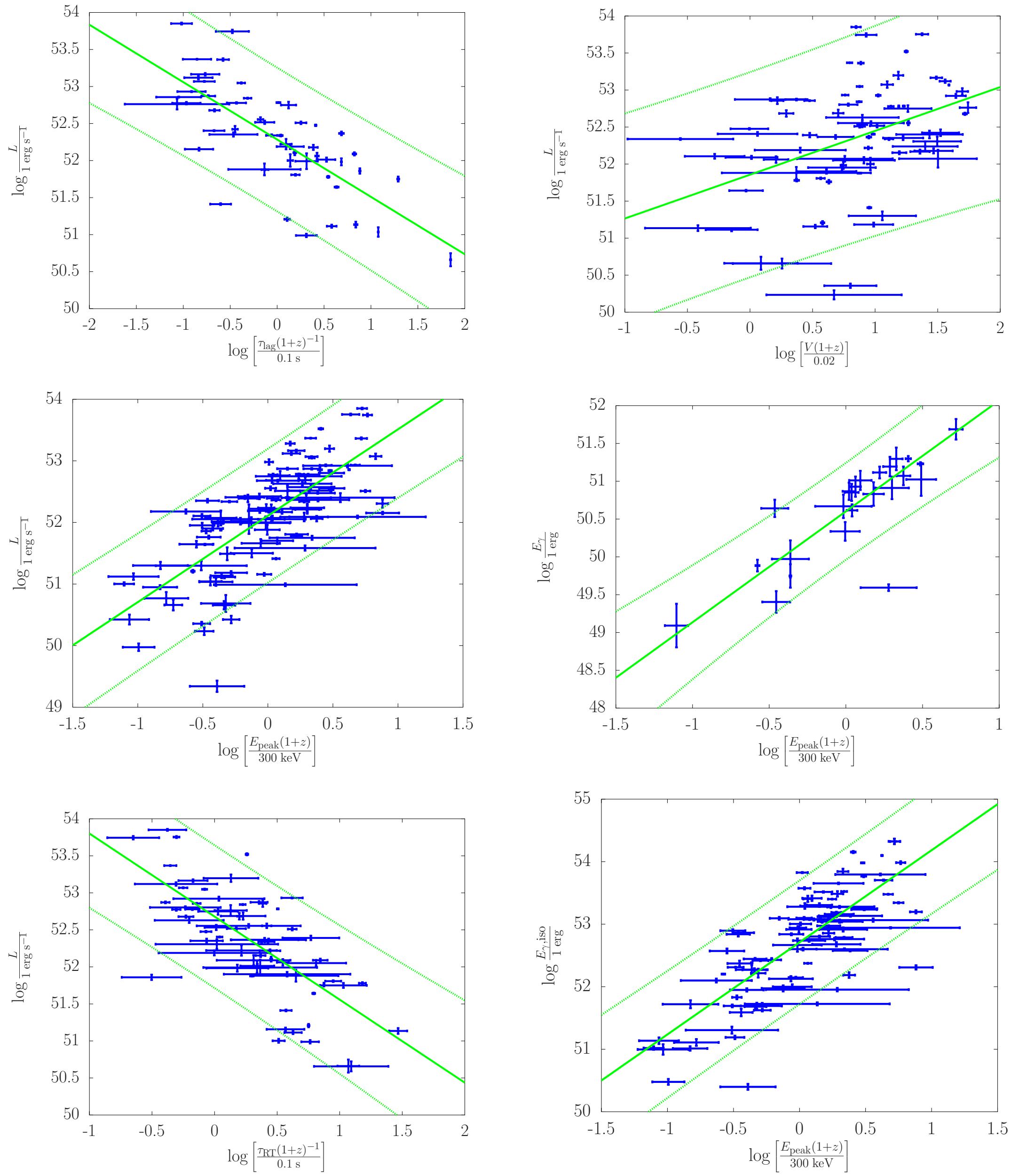

Figure 1. The $\tau_{\rm lag} - L$, $V - L$, $E_{\rm peak} - L$, $E_{\rm peak} - E_\gamma$, $\tau_{RT} - L$ and $E_{\rm peak} - E_{\gamma,\rm iso}$ correlations. The 1σ uncertainties are used as the error bar. The solid lines show the best fit results. The dotted lines plot the 2σ confidence regions.

parametrizations, since independent parameters are introduced in every redshift range and it could, in principle, approach any functional form with the increase of the number of redshift bins (of course, we would need enough observational data to constrain all the parameters well). For a given set of observational data, the parameters w_i are usually correlated with each other, i.e. the covariance matrix

$$\mathbf{C} = \langle \mathbf{w}\mathbf{w}^{\rm T}\rangle - \langle \mathbf{w}\rangle\langle \mathbf{w}^{\rm T}\rangle, \tag{19}$$

is not diagonal. A new set of dark energy EOS parameters $\widetilde{w_i}$ defined by

$$\widetilde{\mathbf{w}} = \mathbf{T}\mathbf{w}. \tag{20}$$

is introduced to diagonalize the covariance matrix. The transformation of $\mathbf{T}$ advocated by Huterer & Cooray (2005) has the advantage that the weights (rows of $\mathbf{T}$) are positive almost everywhere and localized in redshift fairly well, so the uncorrelated EOS parameters $\widetilde{w_i}$ are easy to interpret intuitively. The evolution of the dark energy with respect to the redshift could be estimated from these decorrelated EOS parameters. The transformation of $\mathbf{T}$ is determined as follows. First, we define the Fisher matrix

$$\mathbf{F} \equiv \mathbf{C}^{-1} = \mathbf{O}^{\rm T}\Lambda\mathbf{O}, \tag{21}$$

and then the transformation matrix $\mathbf{T}$ is given by

$$\mathbf{T} = \mathbf{O}^{\rm T}\Lambda^{\frac{1}{2}}\mathbf{O}, \tag{22}$$

Correlation	$z \in [0,1]$	$z \in [1,2]$	$z \in [2,3]$	$z \in [3,8.5]$	Total
$\tau_{\rm lag} - L$	$a = 51.78 \pm 0.13$	$a = 52.47 \pm 0.08$	$a = 52.44 \pm 0.12$	$a = 52.57 \pm 0.24$	$a = 52.28 \pm 0.07$
	$b = -0.55 \pm 0.17$	$b = -0.77 \pm 0.13$	$b = -0.83 \pm 0.21$	$b = -0.60 \pm 0.38$	$b = -0.77 \pm 0.10$
$\sigma_{\rm int}$	0.47 ± 0.11	0.34 ± 0.07	0.36 ± 0.12	0.56 ± 0.26	0.48 ± 0.05
GRB Number	15	19	11	8	53
$V - L$	$a = 51.53 \pm 0.27$	$a = 52.25 \pm 0.24$	$a = 52.38 \pm 0.48$	$a = 53.03 \pm 0.42$	$a = 51.86 \pm 0.15$
	$b = 0.50 \pm 0.44$	$b = 0.35 \pm 0.26$	$b = 0.25 \pm 0.40$	$b = -0.23 \pm 0.33$	$b = 0.59 \pm 0.15$
$\sigma_{\rm int}$	0.78 ± 0.13	0.62 ± 0.10	0.64 ± 0.15	0.50 ± 0.11	0.68 ± 0.06
GRB Number	26	25	15	15	81
$E_{\rm peak} - L$	$a = 51.75 \pm 0.12$	$a = 52.21 \pm 0.10$	$a = 52.27 \pm 0.09$	$a = 52.49 \pm 0.10$	$a = 52.11 \pm 0.05$
	$b = 1.35 \pm 0.23$	$b = 1.29 \pm 0.21$	$b = 1.40 \pm 0.24$	$b = 0.55 \pm 0.26$	$b = 1.40 \pm 0.12$
$\sigma_{\rm int}$	0.63 ± 0.09	0.48 ± 0.08	0.40 ± 0.07	0.43 ± 0.07	0.54 ± 0.04
GRB Number	34	30	27	25	116
$E_{\rm peak} - E_\gamma$	$a = 50.59 \pm 0.10$	$a = 50.66 \pm 0.11$	$\cdots$	$\cdots$	$a = 50.60 \pm 0.07$
	$b = 1.54 \pm 0.21$	$b = 1.55 \pm 0.34$	$\cdots$	$\cdots$	$b = 1.47 \pm 0.20$
$\sigma_{\rm int}$	0.24 ± 0.11	0.14 ± 0.13	$\cdots$	$\cdots$	0.31 ± 0.08
GRB Number	10	7	4	3	24
$\tau_{RT} - L$	$a = 52.49 \pm 0.18$	$a = 52.81 \pm 0.11$	$a = 52.56 \pm 0.18$	$a = 52.86 \pm 0.16$	$a = 52.68 \pm 0.07$
	$b = -1.20 \pm 0.26$	$b = -0.77 \pm 0.21$	$b = -1.03 \pm 0.54$	$b = -0.96 \pm 0.57$	$b = -1.12 \pm 0.14$
$\sigma_{\rm int}$	0.50 ± 0.08	0.39 ± 0.07	0.55 ± 0.16	0.43 ± 0.14	0.48 ± 0.05
GRB Number	25	22	13	12	72
$E_{\rm peak} - E_{\gamma,\rm iso}$	$a = 52.48 \pm 0.13$	$a = 52.84 \pm 0.11$	$a = 52.74 \pm 0.08$	$a = 52.92 \pm 0.10$	$a = 52.71 \pm 0.05$
	$b = 1.47 \pm 0.25$	$b = 1.54 \pm 0.26$	$b = 1.29 \pm 0.21$	$b = 0.89 \pm 0.25$	$b = 1.47 \pm 0.12$
$\sigma_{\rm int}$	0.62 ± 0.10	0.54 ± 0.09	0.36 ± 0.07	0.39 ± 0.07	0.49 ± 0.04
GRB Number	28	26	25	22	101

Table 2. Results of fits to the luminosity correlations for GRBs in each redshift bin and the whole sample.

	$\tau_{\rm lag} - L$	$V - L$	$E_{\rm peak} - L$	$E_{\rm peak} - E_\gamma$	$\tau_{RT} - L$	$E_{\rm peak} - E_{\gamma,\rm iso}$
da/dz	0.22 ± 0.08	0.44 ± 0.15	0.18 ± 0.04	$\cdots$	0.06 ± 0.07	0.09 ± 0.04
db/dz	-0.06 ± 0.12	-0.23 ± 0.15	-0.22 ± 0.10	$\cdots$	0.07 ± 0.18	-0.19 ± 0.10

Table 3. The slopes of the parameters a and b versus redshift.

except that the rows of the matrix $\mathbf{T}$ are normalized such that

$$\sum_j T_{ij} = 1. \tag{23}$$

We divided redshifts at points $z = 0.2, 0.5, 1$ and Markov chain Monte Carlo techniques are used with $O(10^6)$ samples generated for each result. Since current observational data have only very weak constraints on the nature of dark energy at redshifts $z > 1$ (we tried constraining the dark energy EOS without imposing any prior on $w(z > 1)$ using the parameterization described above with GRBs and other data sets, no substantial constraints on the dark energy EOS at redshifts $z > 1$ can be obtained), we simply set $w(z > 1) = -1$, and focus on the dark energy EOS at $z \leqslant 1$.

In addition to GRBs, we have used Union2 compilation of SNe Ia from Amanullah et al. (2010), BAO measurement from Percival et al. (2010) and $\Omega_m h = 0.213 \pm 0.023$ from Tegmark et al. (2004). We assumed the prior $\Omega_k = -0.014 \pm 0.017$ (Spergel et al. 2007) for the cosmic curvature. We also used the $H(z)$ data from Stern et al. (2010) and Riess et al. (2009).

For each luminosity correlation for GRBs, the $\chi^2_{\rm GRB}$ is calculated by

$$\chi^2_{\rm GRB} = -2 \ln L, \tag{24}$$

where L is given by Eq. (17) except that cosmological parameters are free parameters now. For other data set as well as the priors, the usual way of calculating χ^2 is used, i.e., for a physical quantity ξ with experimentally measured value ξ_o, standard deviation σ_ξ, and theoretically predicted value $\xi_t(\theta)$, where θ is a collection of parameters needed to calculate the theoretical value, the χ^2 value is given by

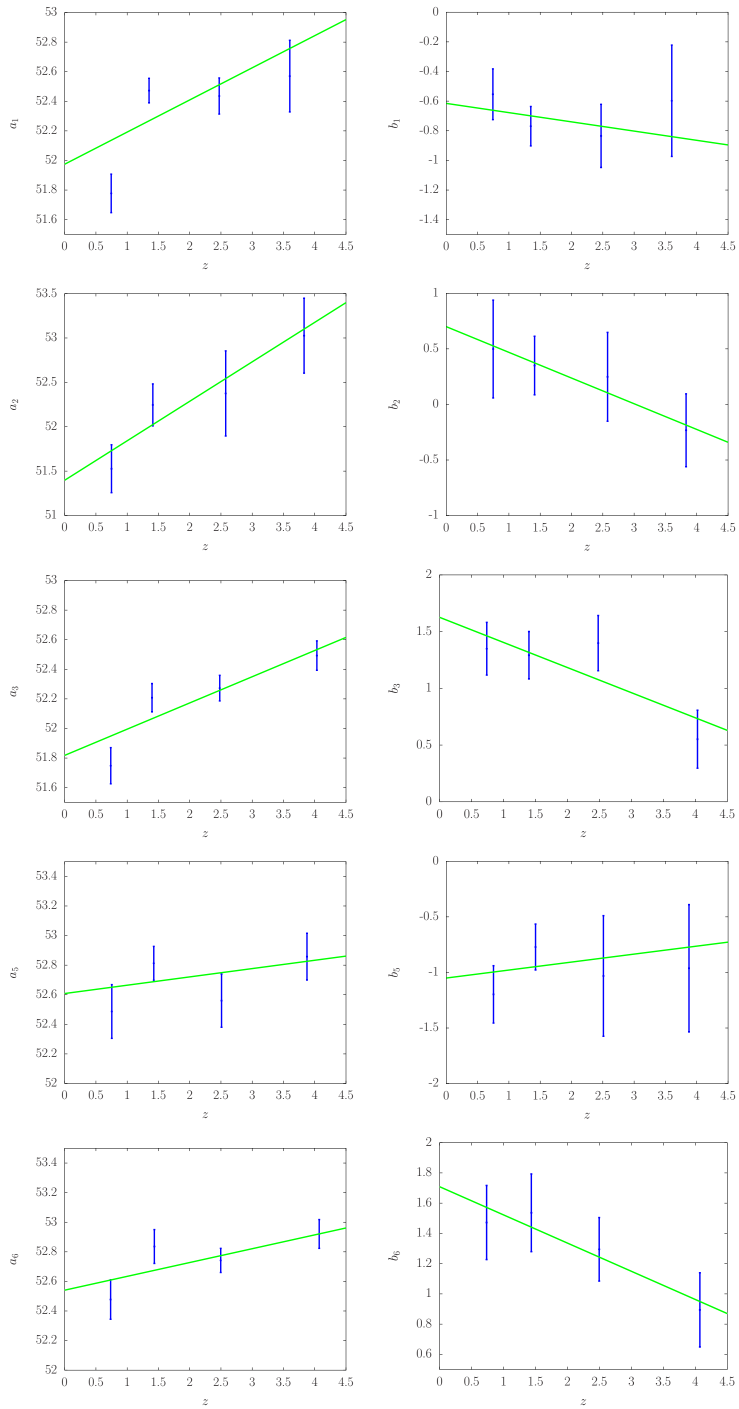

Figure 2. The correlation coefficients a, b obtained in four redshift bins for the five correlations. The $E_{\rm peak} - E_\gamma$ correlation are not included because there are no enough GRBs in each redshift bin for this correlation.

$$\chi^2_\xi(\theta) = \frac{(\xi_t(\theta) - \xi_o)^2}{\sigma^2_\xi}. \qquad (25)$$

The total $\chi^2_{\rm total}$ is the sum of all the χ^2s from independent data.

Figure 3 shows the result derived from the data set described above. We can see that though the dark energy is consistent with the cosmological constant ($w(z) = -1$) at the 2σ confidence level, there is still considerable room for an evolving dark energy EOS. Notably, the slight deviation of the dark energy from the cosmological constant at $z \geqslant 0.5$, which persistently appears with many previous data sets, still exists here. For our result here, the deviation is mainly due to the GRBs. Though the Union compilation of SNe Ia gives the same trend of deviation from the cosmological constant due to the unexpected brightness of the Hubble data at $z > 1$, when the sample is enlarged, it seems

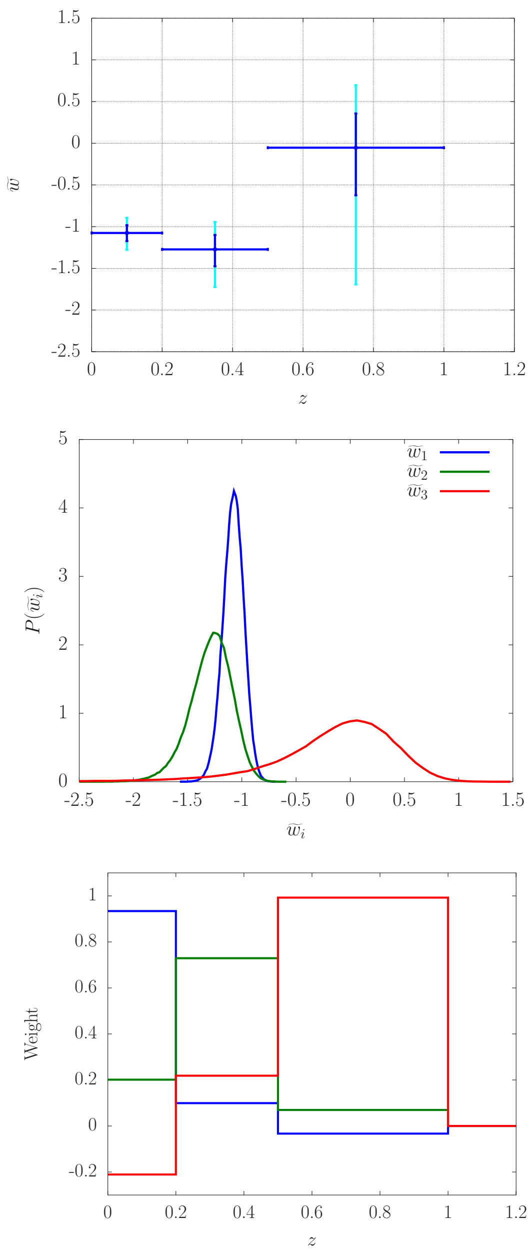

Figure 3. Estimates of the uncorrelated dark energy EOS parameters $\widetilde{w}_i$. Top panel: uncorrelated dark energy parameters versus redshift, in which the vertical errorbars correspond to 1σ and 2σ confidence levels of $\widetilde{w}_i$ and the horizontal errorbars span the corresponding redshift bins from which the contributions to $\widetilde{w}_i$ come most. Middle panel: Probability distribution for $\widetilde{w}_i$. Bottom panel: window functions for $\widetilde{w}_i$.

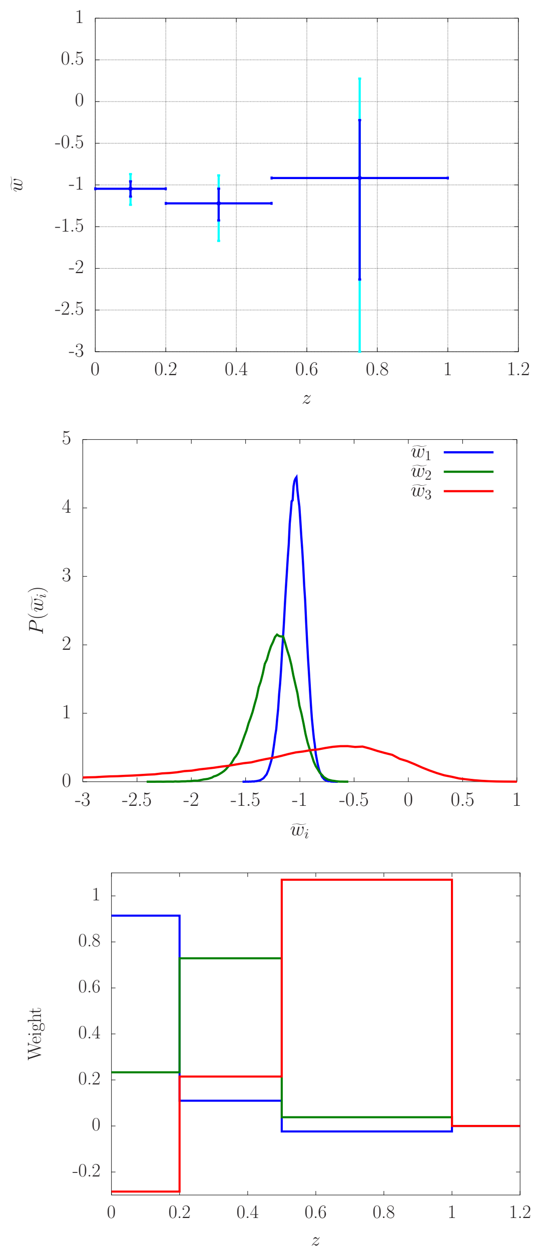

Figure 4. Estimates of the uncorrelated dark energy EOS parameters $\widetilde{w}_i$. Same as the Figure 3 except that GRBs are not included in the fit.

that such a character of the SN Ia data has been averaged out in the Union2 compilation. As a comparison, we also present in Figure 4 the result derived from the data set without GRBs included. See also Wang et al. (2010) and Park et al. (2010) for similar analysis on the nature of the dark energy with Union2 compilation of SNe Ia. The deviation of the dark energy EOS from -1 may arise from many possible reasons, for example, the statistical errors due to the limitation of current observational data, some biasing systematic errors in the observational data (especially there is still some distance to calibrating GRBs as ideal standard candles), or the nature of the dark energy itself, etc. It should be made clear about the cause of the deviation with future observational data in order to understand the dark energy better.

5 CONCLUSIONS

To build up the Hubble diagram to a redshift higher than the one of SNe Ia, most attempts have been devoted to search for a method to make GRBs standardiz-

able candles. Different correlations have been proposed in order to build up a GRB Hubble diagram and constrain cosmological parameters. As a further step, we have here considered the latest GRB dataset and luminosity correlations to constrain the cosmological parameters and dark energy.

In this paper, we derived the six luminosity correlations ($\tau_{\rm lag}-L$, $V-L$, $E_{\rm peak}-L$, $E_{\rm peak}-E_\gamma$, $\tau_{RT}-L$, $E_{\rm peak}-E_{\gamma,\rm iso}$) from the light curves and spectra of the latest 116 long GRBs. We find that the intrinsic scatter of $V-L$ correlation is too large and there seems no inherent correlation between the two parameters using the latest GRB data. The other five correlations indeed exist when enlarging the sample. We have found no statistically significant evidence for the redshift evolution of the luminosity correlations. However, even the best GRB luminosity correlation is currently not competitive with other cosmological probes of the cosmic acceleration expansion since the cosmological parameter 1σ errors derived from GRBs ($\Omega_{\rm m}=0.31^{+0.13}_{-0.10}$) are more than an order of magnitude larger than the corresponding errors obtained using SN Ia standard candles and other geometrical probes. But the estimates of cosmological parameters from GRBs are important because they provide an independent confirmation of the results from other probes.

We also performed an investigation on the dark energy EOS using the GRBs together with the Union2 compilation of SNe Ia and the $H(z)$ data. The result is consistent with the cosmological constant at 2σ confidence level. However, mainly due to the GRB data, the slight deviation of the dark energy EOS from -1 at $z\geqslant 0.5$, which persistently appears with many previous data sets, still exists.

ACKNOWLEDGEMENTS

This work is supported by the National Natural Science Foundation of China (grants 10873009 and 11033002) and the National Basic Research Program of China (973 program) No. 2007CB815404 (for ZGD). SQ is supported by the National Natural Science Foundation of China under grant No. 10973039, the Jiangsu Planned Projects for Postdoctoral Research Funds under grant No. 0901059C and the China Postdoctoral Science Foundation under grant No. 20100471421. FYW is supported by Jiangsu Planned Projects for Postdoctoral Research Funds 1002006B and China Postdoctoral Science Foundation funded project 20100481117.

REFERENCES

Aldering, G., et al. 2004, arXiv:astro-ph/0405232
Amanullah, R. et al. 2010, ApJ, 716, 712
Amati, L., et al. 2002, A&A, 390, 81
Amati L., 2006, MNRAS, 372, 233
Amati, L., et al. 2008, MNRAS, 391, 577
Amati, L., Frontera, F., & Guidorzi, C. 2009, A&A, 508, 173
Astier, P., et al. 2006, A&A, 447, 31
Band, D., et al. 1993, ApJ, 413, 281
Band, D. L., & Preece, R. 2005, ApJ, 627, 319
Basilakos, S., & Perivolaropoulos, L. 2008, MNRAS, 391, 411
Bosnjak, Z., Celotti, A., Longo, F., et al. 2008, 384, 599
Bromm, V., & Loeb, A. 2002, ApJ, 575, 111
Bromm, V., & Loeb, A. 2006, ApJ, 642, 382
Butler, N. R., Kocevski, D., Bloom, J. S., & Curtis, J. L, 2007, ApJ, 671, 656
Butler, N. R., Kocevski, D., & Bloom, J. S. 2009, ApJ, 694, 76
Capozziello, S., & Izzo, L. 2008, A&A, 490, 31
Capozziello, S. & Izzo, L. 2010, A&A, 519, A73
Cardone, V. F., Capozziello, S., & Dainotti M.G. 2009, MNRAS, 400, 775
Cardone, V. F., Dainotti, M.G., Capozziello, S. & Willingale, R., arXiv:1005.0122
Cattoën, C & Visser, M., gr-qc/0703122v3
Ciardi, B., & Loeb, A. 2000, ApJ, 540, 687
D'Agostini, G. 2005, arXiv:physics/0511182
Dai, Z. G., Liang, E. W., &, Xu, D., 2004, ApJ, 612, L101
Dainotti, M. G., Cardone, V. F., & Capozziello, S. 2008, MNRAS, 391, L79
Dainotti, M. G., et al. 2010, ApJ, 722, L215
Eisenstein, D. J., et al. 2005, ApJ, 633, 560
Fenimore, E. E., &, Ramirez-Ruiz, E., 2000, (arXiv:astro-ph/0004176)
Friedman, A. S., & Bloom, J. S. 2005, ApJ, 627, 1
Gao, H., Liang, N., & Zhu, Z. H. arXiv:1003.5755v2
Ghirlanda, G., Ghisellini, G., &, Lazzati, D., 2004a, ApJ, 616, 331
Ghirlanda, G., Ghisellini, G., &, Lazzati, D., 2004b, ApJ, 613, L13
Ghirlanda, G., Ghisellini, G., Firmani, C., Celotti, A., & Bosnjak, Z. 2005, MNRAS, 360, 45
Ghirlanda, G., et al. 2007, A&A, 466, 127
Ghirlanda, G., et al. 2008, MNRAS, 387, 319
Huterer, D., & Cooray, A. 2005, Phys. Rev. D, 71, 023506
Izzo, L. et al. 2009, A&A, 508, 63
Komatsu, E., et al., 2009, ApJS, 180, 330
Krimm, H. A., Yamaoka, K., Sugita, S., et al. 2009, ApJ, 704, 1405
Lamb, D. Q., & Reichart, D. E. 2000, ApJ, 536, 1
Li, L. X., 2007, MNRAS, 379, L55
Liang, E. W., & Zhang, B. 2005, ApJ, 633, 611
Liang, E. W., & Zhang, B. 2006, MNRAS, 369, L37
Liang, N., Xiao, W. K., Liu, Y., & Zhang, S. N. 2008, ApJ, 685, 354
Liang, N., Wu, P. X., & Zhang, S. N. 2010, Phys. Rev. D., 81, 083518
Liang, N. & Zhu, Z. H., 2010, arXiv:1006.1105
Nakar, E., & Piran, T. 2005, MNRAS, 360, L73
Nava, L., Ghirlanda, G., Ghisellini, G., Firmani, C. 2008, MNRAS, 391, 639
Norris, J. P., Marani, G. F., &, Bonnell, J. T. 2000, ApJ, 534, 248
Park, J., Park, C. & Hwang, J. 2010, arXiv: 1011.1723
Percival W. J., et al. 2010, MNRAS, 401, 2148
Perlmutter, S., et al., 1999, ApJ, 517, 565
Qi, S. & Lu, T., 2010, ApJ, 717, 1274
Qi, S., Wang, F. Y.,&, Lu, T., 2008a, A&A, 483, 49
Qi, S., Wang, F. Y.,&, Lu, T., 2008b, A&A, 487, 853
Qi, S., Lu, T., &, Wang, F. Y., 2009, MNRAS, 398, L78
Riess, A. G., et al., 1998, AJ, 116, 1009
Riess, A. G., et al. 2007, ApJ, 659, 98
Riess, A. G., et al. 2009, ApJ, 699, 539
Salvaterra, R., et al. 2009, Nature, 461, 1258
Schaefer, B. E., 2003, ApJ, 583, L67
Schaefer, B. E., 2007, ApJ, 660,16

Stern, D. et al. 2010, JCAP, 2010, 2, 8
Spergel, D. N. et al., 2007, ApJS, 170, 377
Sullivan, S., Cooray, A., & Holz, D. E. 2007, JCAP, 0709, 004
Tanvir, N. R., et al. 2009, Nature, 461, 1254
Tegmark M. et al., 2004, ApJ, 606, 702
Tegmark M. et al., 2006, Phys. Rev. D., 74, 123507
Visser, M. 2004, Class. Quant. Grav., 21, 2603
Vitagliano, V. et al. 2010, JCAP, 03, 005
Wang, F. Y., &, Dai, Z. G., 2006, MNRAS, 368,371
Wang, F. Y., Dai, Z. G., & Zhu, Z. H. 2007,ApJ, 667, 1
Wang, F. Y., Dai, Z. G., & Qi, S. 2009a, RAA, 9, 547
Wang, F. Y., Dai, Z. G., & Qi, S. 2009b, A&A, 507, 53
Wang, S., Li, X. D. & Li, M. 2010, arXiv: 1009.5837
Wang, Y. 2008, Phys. Rev. D., 78, 123532
Wei, D.M. & Gao, W.H., 2003, MNRAS, 345, 743
Wright, E. L. 2007, ApJ, 664, 633
Xiao, L. M. & Schaefer, B. E. 2009, ApJ, 707, 387
Yu, B., Qi, S. & Lu, T., 2009, ApJ, 705, L15